Characterization of molecular alignment in aqueous suspensions of Pf1 bacteriophage

Markus Zweckstetter & Ad Bax
Laboratory of Chemical Physics, National Institute of Diabetes and Digestive and Kidney Diseases, National Institutes of Health, Bethesda, MD 20892-0520, U.S.A.

Abstract

The phase diagram of Pf1 solutions has been studied indirectly by observation of ^{2}H quadrupole splittings of the solvent signal and measurement of dipolar couplings in solute macromolecules. At low volume fractions of Pf1 and at high ionic strength, alignment of both the phage and the solute depends strongly on the strength of the magnetic field. Both the theoretical and experimentally determined phase diagram of Pf1 show that at low concentrations and high ionic strengths the solution becomes isotropic. However, just below the nematic phase boundary the behavior of the system is paranematic, with cooperative alignment which depends on the strength of the applied magnetic field. Above 16 mg/ml Pf1 is fully nematic up to 600 mM NaCl. Alignment of proteins with a significant electric dipole moment, which tends to be strong in Pf1, can be reduced by either high ionic strength or low phage concentration. Because ionic strength modulates both the orientation and magnitude of the alignment tensor in Pf1 medium, measurement at two ionic strengths can yield linearly independent alignment tensors.

Introduction

Residual dipolar couplings (rdc) can be observed in a macromolecule when dissolved in a dilute liquid crystalline medium (Tjandra and Bax, 1997). Provided alignment is sufficiently weak, such that homonuclear ^{1}H-^{1}H dipolar couplings remain smaller than or comparable to typical J_{HH} values, measurement of residual one-bond heteronuclear couplings is quite straightforward (Tolman et al., 1995). Such rdc's constrain the orientations of internuclear vectors relative to a molecule's alignment tensor. This information is very useful for improving NMR structure determination, and also offers new ways for structure validation, distinguishing monomeric from multimeric structures, determination of relative domain orientation, and evaluation of flexibility in multi-domain proteins (Tjandra et al., 1997; Cornilescu et al., 1998; Clore and Garrett, 1999; Skrynnikov et al., 2000; Zweckstetter and Bax, 2000).

Much effort has been directed towards development of ordering media that are stable over a wide range of pH and temperature and that have a minimal adverse effect on rotational diffusion (Cavagnero et al., 1999; Ottiger and Bax, 1999; Fleming et al., 2000; Ruckert and Otting, 2000; Barrientos et al., 2001). Availability of multiple media is particularly useful as it allows for measurement of rdc's in different alignment frames (Ramirez and Bax, 1998; Al-Hashimi et al., 2000). The combination of disc-shaped bicelles (Sanders and Schwonek, 1992) and rod-shaped virus particles is particularly useful in this regard (Clore et al., 1998). Two different mechanisms of interaction, steric for nearly neutral bicelles and primarily electrostatic for phage, generally result in linearly independent alignment tensors (Sass et al., 1999). However, both systems also have their drawbacks. The bicelle liquid crystalline phase is unstable in the presence of certain proteins and offers only a limited temperature range (Ottiger and Bax, 1998). Phage particles are highly negatively

charged and can bind non-specifically to macromolecules that have a significant positively charged surface patch. This not only results in excessive alignment, but can also shorten the transverse relaxation time and thereby the inherent resolution and sensitivity of multi-dimensional NMR experiments. Lowering the phage concentration to 1–2 mg/ml reduces the degree of induced order, but does not necessarily solve the line broadening problem (Ojennus et al., 1999).

Here, we characterize alignment of macromolecules in low volume fractions of Pf1 as a function of ionic strength. Use of this Pf1-based liquid crystal for macromolecule alignment was first demonstrated by Pardi and co-workers (Hansen et al., 1998), and it has become one of the most widely used media for this purpose. We show that below the nematic threshold concentration, but above the isotropic coexistence concentration, Pf1 solutions are paranematic. This region is still very useful for alignment of solute macromolecules, but the induced degree of order depends strongly on ionic strength, Pf1 concentration, and the strength of the magnetic field.

Theory

The theory for the phase behavior of highly anisometric particles such as Pf1 was first developed by Onsager (Onsager, 1949). It predicts the concentration at which a solution undergoes a spontaneous first order phase transition from an isotropic to a chiral nematic phase (Torbet and Maret, 1981). Onsager's theory, based on the second virial coefficient in the Helmholtz free energy expansion, subsequently has been extended to include flexibility of rods (Khokhlov and Semenov, 1982; Odijk, 1986). Stroobants et al. (1986) further refined the theory by introducing a twisting factor, which accounts for the fact that electrostatic repulsion favors a twisted relative orientation of charged rods.

Onsager suggested that if the product $B_2 c_p$ of the second virial coefficient B_2 (effective volume) and the number density of rods c_p is greater than a certain cutoff value, the solution will be anisotropic. Because of the first-order character of the isotropic-nematic transition, there is a density regime $c_p \in [c_i, c_a]$, where an isotropic phase coexists with a nematic phase. Numerical results for the isotropic and anisotropic coexistence concentration c_i and c_a in case of rigid rods are

$$c_i = 3.290[(1 - 0.675h)B_2]^{-1}$$
$$c_a = 4.191[(1 - 0.730h)B_2]^{-1} \tag{1a}$$

and for semi-flexible rods

$$c_i = 0.3588[(1 - \sqrt{x})B_2]^{-1}$$
$$c_a = 0.3588[(x - \sqrt{x})B_2]^{-1} \tag{1b}$$

with $x = 0.8648 + 0.0091h$ (Odijk, 1986; Vroege, 1989). The twist parameter h takes into account that due to electrostatic repulsion a perpendicular orientation of particles is favored (Stroobants et al., 1986). 'Semi-flexible' describes chains that are locally stiff, but are so long that they can still form coils with $L \gg P \gg D_{eff}$, where P is the persistence length, L the contour length (which is the rod length measured along its curved axis), and D_{eff} the effective rod diameter (Khokhlov and Semenov, 1981, 1982). The second virial coefficient B_2 corresponds to an effective volume and is given by (Stigter, 1977)

$$B_2 = \pi D_{eff} L^2 / 4 \tag{2}$$

where

$$D_{eff} = D + \kappa^{-1}(\ln \omega + 0.7704) \tag{3}$$

with κ being the Debye-Hueckel inverse length. D_{eff} takes into account that the isotropic-anisotropic transition in a solution of rigid polyelectrolyte rods is influenced by the effective increase in rod diameter relative to its hard-cylinder value D as the ionic strength decreases. The contact potential ω is given by (Stigter, 1982)

$$\omega = 2\pi Z^2 [\beta\gamma x_0 K_1(x_0)]^{-2} Q \kappa^{-1} \exp(-2x_0). \tag{4}$$

In this equation, Z is the charge per unit length along the cylinder axis, $Q = e^2/\varepsilon k_B T$ the Bjerrum length with ε the dielectric constant, x_0 the radius in units of κ^{-1} (i.e., $x_0 = \kappa D/2$), and $K_1(x_0)$ the modified Bessel function. The factors β and γ are corrections to the Debye-Hueckel charge-potential and potential-distance relations, tabulated in terms of x_0 and ξ/x_0 where $\xi = ZQ$ (Stigter, 1982). For systems with a rather high concentration of highly charged polyelectrolytes ($\xi > 1$), the contribution of the polyions to the ionic strength is taken into account by an effective inverse Debye radius of

$$\kappa = 8\pi Q(c_s + \Gamma z_p c_p) \tag{5}$$

where c_s is the concentration of added monovalent salt and z_p the polyion valence ($\sim 19\,100$) (Sato and Teramoto, 1991). Γ denotes the Donnan salt exclusion coefficient, which is given by (Manning, 1987)

$$\Gamma = (4\xi)^{-1}. \tag{6}$$

For rigid rods, and neglecting both the effect of the twist parameter h and the contribution of Pf1 to the ionic strength, the standard deviation, σ, of the distribution width of rods relative to the liquid crystal director axis is given by (Kassapidou et al., 1995)

$$\sigma = \pi^{1/2}/2(B_2 c_p)^{-1}. \tag{7}$$

The above equations summarize the phase behavior of long, charged rods.

The persistence length of the phages *fd* and M13 is about 2000 nm (Song et al., 1991). The Pf1 persistence length is reportedly comparable to that of *fd* and M13 (Dogic and Fraden, 1997), but the Pf1 contour length is considerably longer (1960 nm) (Zimmermann et al., 1986), i.e., comparable to its persistence length. Thus, the phase behavior for Pf1 is expected to fall in between that predicted for rigid rods and semi-flexible rods.

Materials and methods

Pf1 phage was purchased from ASLA Ltd., Riga, Latvia (ASLA http://130.237.129.141//asla/asla-phage. htm). Phage concentrations were adjusted by weighing appropriate amounts of a 50 mg/ml stock solution and verified by UV absorbance at 270 nm using an extinction coefficient, $\varepsilon = 2.25 \text{ cm}^{-1} \text{ mg}^{-1}$ ml (Kostrikis et al., 1994). Due to the high viscosity of phage solutions, errors in Pf1 concentration are estimated at ca. 5%. Protein was recovered from Pf1 samples, usually at high salt, by centrifugation at 436 000 *g* for 1 h at 30° in a Beckman TL-100 tabletop ultracentrifuge.

$^{13}C/^{15}N$-enriched human ubiquitin was purchased from VLI Research, Southeastern, PA. $^{13}C/^{15}N/^2H$-enriched ubiquitin was prepared as described by Sass et al. (1999) and kindly provided by S. Grzesiek. ^{15}N-enriched RecA binding protein DinI and ^{15}N-enriched first Ig-binding domain of Streptococcal protein G (further simply referred to as protein G) were prepared as described previously (Ramirez et al., 2000; Gronenborn et al., 1991). NMR samples contained 0.2 mM ubiquitin, 0.3 mM DinI and 0.2 mM protein G domain in 90% H_2O/10% D_2O. Temperature studies on fully aligned Pf1 were carried out using a selectively $^{13}C/^{15}N$ labeled dodecamer, d(CGCGAATTCGCG)$_2$ (Tjandra et al., 2000) with the labeled nucleotides indicated by underlines, in 10 mM sodium phosphate (pH = 6.8) and 50 mM KCl. Temperature studies in nearly isotropic conditions were carried out using a 1 mM $^2H/^{13}C/^{15}N$-labeled ubiquitin sample in 240 mM NaCl (pH = 7.3) and 3.9 mg Pf1/ml.

All NMR experiments were carried out in thin-wall Shigemi microcells (Shigemi Inc., Allison Park, PA) on Bruker DMX500, DRX600, DMX750 and DRX800 spectrometers equipped with three-axes pulsed field gradient $^1H/^{15}N/^{13}C$ probeheads. Quadrupole splittings of the solvent ^2H resonance were measured after sufficient equilibration of the NMR samples in the magnet was reached (less than 1% change over 15 min). No ^2H line broadening with increasing salt concentration was observed. Residual ^{15}N-^1H dipolar couplings were derived from IPAP [$^{15}N,^1H$]-HSQC experiments (Ottiger et al., 1998) using NMRPipe/NMRDraw (Delaglio et al., 1995) and analyzed with the program PALES (Zweckstetter and Bax, 2000). Average values of ^{15}N $T_{1\rho}$ relaxation times for $^2H/^{13}C/^{15}N$-enriched ubiquitin were determined by comparing first t_1 increments of a two-dimensional ^{15}N $T_{1\rho}$-experiment (Peng et al., 1991). ^{15}N spin-lock pulses of 2 ms and 120 ms (or 160 ms) length were applied at an RF field strength of 2.0 kHz, carrier position 117.8 ppm, and a temperature of 25 °C. No corrections for off-resonance effects were applied.

Calculation of liquid crystal phase parameters of Pf1 phage, based on a theory for lyotropic nematic liquid crystals of rod-like polymer chains, was done with Mathematica. All calculations used a Pf1 contour length of 1960 nm and a 6.7 nm diameter (Liu and Day, 1994). Pf1 is negatively charged at pH 7.4, with an approximate linear charge density of 10 e/nm, and has a molecular weight of 3.75×10^7 g/mol (Zimmermann et al., 1986).

Results and discussion

As discussed in the section Theory, lyotropic liquid crystals phase separate into an isotropic and a nematic region once the nematogen concentration is reduced below the nematic threshold concentration, c_a. When the concentration is lowered further, such that the average concentration reaches the nematogen concentration in the isotropic region of the sample, c_i, the entire sample turns isotropic. Because $c_a > c_i$, and the density of most nematogens is higher than for the solvent, the average density of the nematic region is higher than for the isotropic region and gravity causes it to occupy the bottom region of the sample. Visually such phase separation can be observed very clearly for many systems, including solutions containing bacteriophage *fd* or tobacco mosaic virus (TMV)

(Clore et al., 1998), cellulose crystallites (Fleming et al., 2000), and various other rod shaped particles. For Pf1, the c_a concentration at low ionic strength is very low, however, and macroscopic phase separation does not readily occur, making experimental detection less straightforward. Here, we evaluate the Pf1 phase diagram both computationally, and by two separate experimental methods.

Predicted phase behavior of Pf1

Figure 1 shows how the second virial coefficient, B_2, changes as a function of ionic strength. The plotted value actually corresponds to B_2c_p, where the number concentration c_p is adjusted to correspond to 12 mg Pf1/ml. The precise B_2c_p value at which the Pf1 medium is expected to become fully nematic depends on the flexibility of monodispersed Pf1. Fully accounting for Pf1 flexibility would require the Helmholtz free energy to be minimized numerically (Odijk, 1986). Instead, we consider two extreme cases, the rigid-rod limit and the very long coil limit, for which $B_2c_p > 4.19$ and $B_2c_p > 5.51$ is required for nematic behavior, respectively (Herzfeld et al., 1984; Lekkerkerker et al., 1984; Vroege and Odijk, 1988). Including a twist factor, h = 0.15, raises the nematic threshold B_2c_p values by about 10% to 4.66 and 5.56 for the rigid-rod and flexible chain model, respectively (cf., Equation 1). In these calculations, the effective diameter, D_{eff}, was calculated assuming a surface charge density of 10 e/nm. Note, however, that D_{eff} becomes rather insensitive to the precise value of the charge density above 5 e/nm (Tang and Fraden, 1995).

At the lowest ionic strength, B_2c_p for the 12 mg/ml Pf1 solution is calculated to be an order of magnitude above the nematic coexistence concentration, independent of the model employed (Figure 1). However, with increasing ionic strength B_2c_p rapidly decreases. At a salt concentration of 520 mM, B_2c_p approaches or drops below the calculated nematic coexistence concentration for the rigid-rod and long-coil model, respectively. These calculations show that at Pf1 concentrations of 10–20 mg/ml and salt concentrations above 50 mM one approaches the regime where the aqueous Pf1 solutions are no longer nematic.

Centrifugation-assisted phase separation

As mentioned above, at low ionic strength Pf1 remains nematic down to very low concentrations, and gravity can be insufficient for inducing a clean separation of isotropic and nematic phases once the concentration is
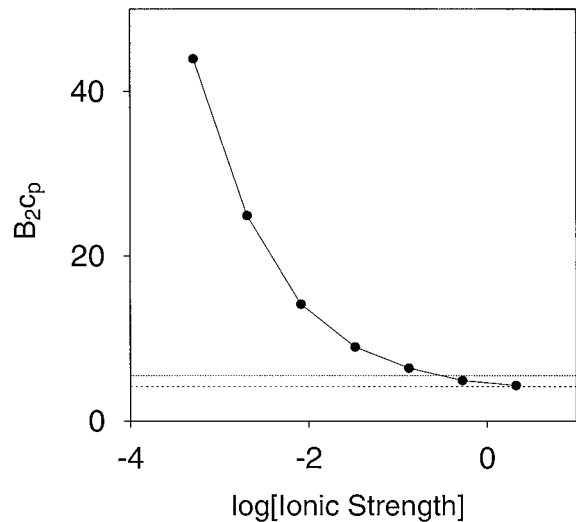

Figure 1. Calculated B_2c_p value as a function of ionic strength for 12 mg/ml Pf1, and a rigid-rod diameter of 6.7 nm. The dashed and dotted horizontal lines mark the nematic coexistence concentrations for a rigid-rod model and a very long coil model, respectively. The twist parameter h is smaller than 0.15 for the complete range of salt concentrations. Including a twisting effect of h = 0.15 raises the nematic coexistence concentration by about 10%, to 4.66 and 5.56, for the rigid-rod and flexible chain model, respectively.

lower than c_a. For the experiments discussed below, low-speed centrifugation, corresponding to 30 g, was used to accelerate the separation and to ensure that the nematic fraction occupied the lower volume fraction in the cell. Four separate fully nematic samples were prepared at ionic strengths of 8, 33, 130 and 520 mM NaCl. These samples were diluted in steps of about 10% and after each step the samples were subjected to 4–16 h of low-speed centrifugation. At Pf1 concentrations above about 7 mg/ml, phase separation can readily be observed using crossed polarizers. At lower concentrations a cross-polarized optical microscope was also used. Isotropic and anisotropic coexistence concentrations were determined by measuring UV absorbance of 50-fold diluted small aliquots (∼4 µl) taken from the isotropic and the nematic fractions at the top and the bottom of the same sample, respectively. All phase separation measurements were carried out at room temperature and pH 7.3. Similar to *fd*, the Pf1 coexistence concentrations are expected to be a function of temperature too (Tang and Fraden, 1996), but we did not study this dependence.

Results of the phase separation experiments are shown in Figure 2. The solid lines mark the calculated isotropic and nematic coexistence concentrations for the rigid rod model, whereas the dashed lines
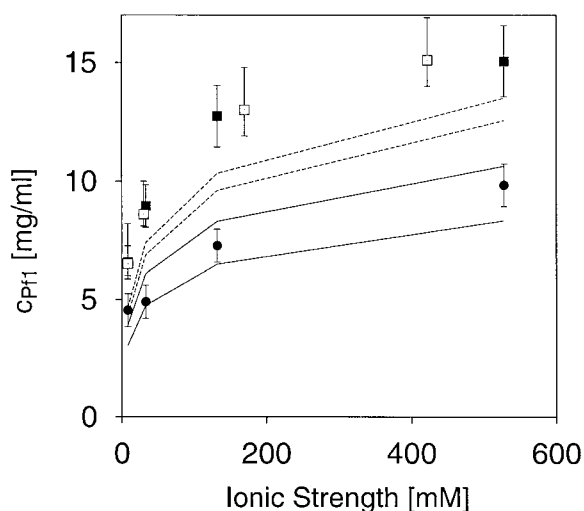
Figure 2. Experimental and predicted phase behavior of Pf1 as a function of ionic strength. Experimental coexistence concentrations measured using the slow centrifugation phase separation procedure are marked by solid symbols (●, isotropic; ■, chiral nematic); the Pf1 concentration at which alignment at 14.1 and 18.8 Tesla becomes field-dependent are marked by open squares (□). Coexistence concentrations calculated from Equations 1–6, using a salt-dependent effective diameter D_{eff} and twisting parameter h, are shown for the rigid-rod model (solid lines) and the very long coil model (dashed lines). In each case, the upper of the two lines corresponds to the nematic coexistence concentration and the lower one to the isotropic coexistence concentration.

correspond to the coexistence concentrations for the semi-flexible rod model. As can be seen in the figure, experimentally we find 20–40% higher values for the nematic threshold concentration than predicted by the calculations, whereas the isotropic threshold falls between values predicted by the rigid and semi-flexible rod models.

The above described phase separation was accomplished with the use of slow speed centrifugation, and it therefore is unclear to what extent centrifugation may be responsible for the higher-than-predicted nematic threshold concentration. Also, we found that the rate at which samples separate varied for different batches of stock solution, even though from an NMR perspective these different stocks behaved indistinguishable. This may relate to very subtle differences in the homogeneity of the Pf1 phage particles. However, these subtle differences had no observable effect on the behavior of the nematic phase as determined from ^{2}H quadrupole splittings of the solvent, or dipolar couplings in a solute macromolecule.

NMR observed nematic phase boundary

In order to address the issue whether centrifugation is responsible for the higher than expected nematic phase boundary concentration we studied this threshold concentration also by NMR, using a different approach. For a fully nematic phase, the degree of alignment is independent of field strength above a typically very low threshold. So, by observing the concentration at which the degree of alignment becomes dependent on the strength of the magnetic field, information can be obtained about the nematic threshold concentration, c_a.

Four fully nematic Pf1 samples, containing 9, 30, 170 and 422 mM NaCl were diluted (at constant ionic strength) in 1 mg/ml steps, and for each step the ^{2}H splitting was recorded at 600 and 800 MHz at 25 °C, pH 7.2. In the nematic phase, the ^{2}H quadrupole splitting at the two fields is highly reproducible with a rms difference of less than 0.2 Hz. The Pf1 concentration at which the ^{2}H splitting differs by more than 0.25 Hz between 600 and 800 MHz is taken as the critical concentration for full alignment. As can be seen in Figure 3, this point approximately coincides with the inflection point below which the ^{2}H splitting is no longer linearly proportional to Pf1 concentration. The slight deviation from linearity just above the coexistence region is caused by a decrease in liquid crystal order upon approaching the phase boundary (Oldenbourg et al., 1988). The induced nematic behavior below the c_a threshold had long been predicted theoretically (Hanus, 1969; Khokhlov and Semenov, 1982) but was first observed only a decade ago, for *fd* (Tang and Fraden, 1993). This first order phase transition is induced by the external magnetic field and results in a so-called paranematic phase, which for Pf1 is found to extend over a wide concentration range.

For all four ionic strengths, the Pf1 nematic threshold concentrations determined in the manner described above are in excellent agreement with the phase separation results (Figure 2). This indicates that the higher-than-expected c_a concentration is not an experimental artifact resulting from slow-speed centrifugation.

As can be seen in Figure 2, the calculated isotropic and nematic Pf1 coexistence concentrations exhibit the same steep dependence on ionic strength as observed experimentally. The isotropic threshold concentration falls between that predicted for the flexible and rigid rod models. However, the theoretical nematic threshold concentration underestimates the experimentally observed one by 20–35%. As a result,
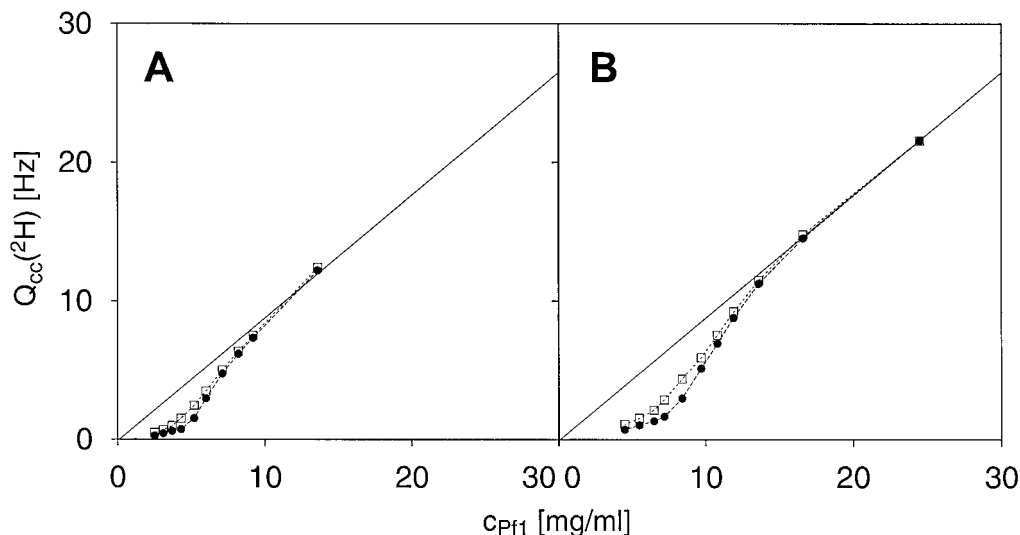
Figure 3. Residual ^{2}H quadrupole coupling $Q_{cc}(^2H)$ of a 90% H_2O/10% D_2O sample as a function of Pf1 concentration, c_{Pf1}, for (A) 9 mM NaCl, and (B) 230 mM NaCl. Spectra were recorded at $B_0 = 14.1$ T (●) and $B_0 = 18.8$ T (□), 25 °C, pH 7.2. The solid line corresponds to $Q_{cc}(^2H) = 0.886 * c_{Pf1}$ (Hansen et al., 2000), and marks the relationship between Pf1 concentration and ^{2}H splitting for fully aligned samples. Pf1 concentrations are calculated from dilution volumes relative to the full alignment value at 24.5 mg Pf1/ml. Therefore, relative errors in Pf1 concentrations are very small (<3%). Overall the curves might be offset by ∼5%, which is the estimated accuracy obtainable for the concentration of the 24.5 mg/ml sample by UV absorbance. Random errors in ^{2}H splittings are less than ∼0.15 Hz.

the experimentally observed coexistence width, $(c_a - c_i)/c_i$, is considerably wider than predicted from the calculations. The nematic coexistence concentration calculated for *fd* also underestimated the experimentally observed one and predicted a coexistence width that was smaller than observed (Tang and Fraden, 1995). Tang and Fraden attributed this difference to the twisting effect, which was not taken into account in their theoretical *fd* calculations. Our calculations for Pf1 include the twisting effect, but nevertheless the coexistence width also remains larger than calculated.

Phage *fd* has half the contour length of Pf1, and Equations 1 and 2 therefore predict that the coexistence number densities for Pf1 are one quarter those of *fd*, assuming the same flexibility. So, in mg/ml the Pf1 coexistence concentrations are predicted to be about half those of *fd*. The above reported numbers for Pf1 therefore agree quite well with the previously reported c_a of about 12 mg/ml for *fd* at 10 mM NaCl, and 25 mg/ml at 100 mM NaCl (Tang and Fraden, 1995).

Paranematic phase region

As discussed above, below the nematic threshold concentration, alignment of phage becomes dependent on the strength of the magnetic field. High degrees of Pf1 alignment can be obtained in this paranematic region,

and this therefore remains very useful for measuring dipolar couplings in solute macromolecules.

The ^{2}H quadrupole splitting was mapped carefully over a wide Pf1 concentration range at two salt concentrations, 9 mM and 230 mM. As each dilution series, starting from 25 down to 2.5 and 4.5 mg/ml Pf1, required numerous steps of sample removal, dilution, mixing and reinsertion in the NMR sample tube, a second control experiment was performed where the sample was diluted in only three steps. Results of this three-step procedure are indistinguishable from the results shown in Figure 3, indicating that losses or damage of Pf1 resulting from sample handling are negligible.

The paranematic behavior of Pf1 is observed over a range that covers the isotropic to the nematic coexistence concentration. If Pf1 behavior were truly monomeric, the order of individual phage particles resulting from their anisotropic diamagnetic susceptibility, $\Delta\chi$, would scale with the square of the magnetic field, provided $\Delta\chi B_0^2/2\mu_0 \ll kT$, with B_0 being the magnetic induction in Tesla, μ_0 the permeability of vacuum ($4\pi \times 10^{-7}$ Tesla^2 m^3 joule^{-1}), k Boltzmann's constant, and T the absolute temperature (Bothner-By, 1996). However, at the Pf1 isotropic threshold concentration of 4.3 mg/ml (10 mM NaCl), the ratio in solvent ^{2}H quadrupole splitting at 11.7 and 18.8 Tesla
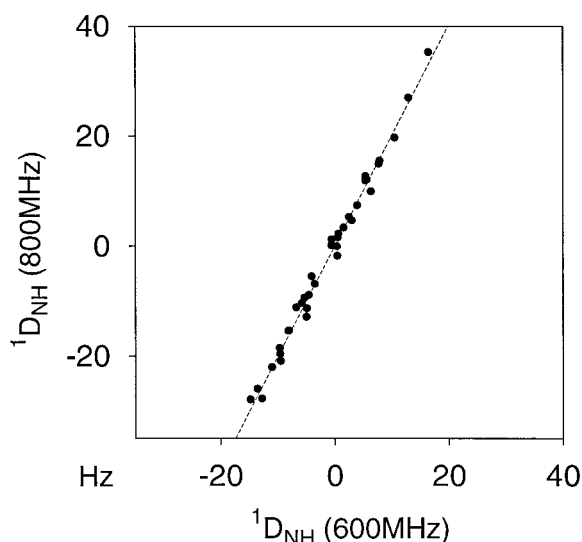
Figure 4. $^1D_{NH}$ splittings in ubiquitin at 800 *versus* 600 MHz. The Pf1 concentration was 4.3 mg/ml at 25 °C, 10 mM NaCl, pH 7.2. The dashed line corresponds to $^1D_{NH}$ (800 MHz) = 2.02 × $^1D_{NH}$ (600 MHz).

Figure 5. ^2H splitting, $Q_{cc}(^2H)$, as a function of NaCl concentration, c_{NaCl}, at 500 MHz (●), 600 MHz (○) and 800 MHz (△). The Pf1 concentration was 12 mg/ml, pH 6.8, 25 °C.

equals 2.0. This is above the ratio of 1.78 expected for quadratic behavior. Similarly, when measuring dipolar couplings for ubiquitin at these two magnetic fields, the same increase is observed (Figure 4). These observed quadrupolar and dipolar splittings at 14.1 Tesla are 20% relative to what would be expected for a fully aligned nematic sample at the same concentration. So, even at the isotropic threshold concentration a small degree of paranematic behavior can still be observed. As can be seen in Figure 3, the paranematic alignment increases gradually until it reaches full alignment at the nematic threshold concentration.

Ionic strength dependence of paranematic phase

As mentioned above, the Pf1 phase diagram is a strong function of ionic strength. This ionic strength dependence of Pf1 alignment is particularly pronounced in the paranematic phase. Results summarized in Figure 5 show that at 12 mg Pf1/ml the nematic order, as monitored by the quadrupole splitting of the ^2H resonance, decreases approximately linearly with the salt concentration. When the NaCl concentration is increased from 10 to 500 mM at $B_0 = 11.7$ T, the ^2H quadrupole coupling reduces to 35% of its value in the fully aligned state. At salt concentrations below 100 mM, the sample is fully nematic and alignment might be expected to be independent of the magnetic field strength. Nevertheless, as will be discussed be-
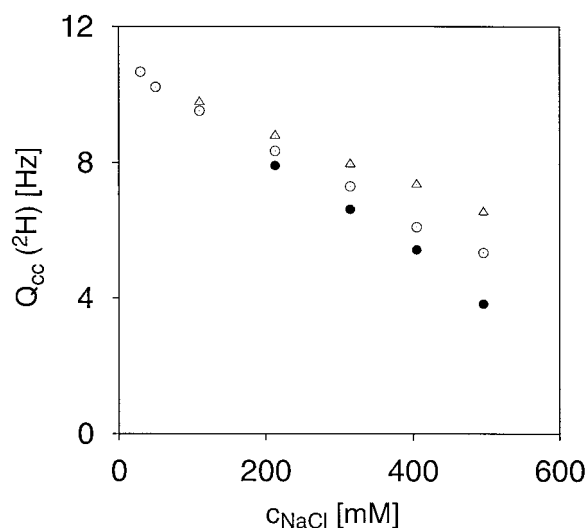
low, a small decrease in alignment with increasing ionic strength is observed in this region. Within the paranematic region, the decrease in quadrupole splitting relative to the splitting expected if the sample were fully nematic, scales approximately with the inverse of the magnetic field (Figure 5).

Theoretical calculations (Equation 7) indicate that the tilt angle distribution width of individual Pf1 rods with respect to the nematic axis increases with ionic strength (Figure 6). The initial decrease in Pf1 order, visible in Figure 5 for salt concentrations below 100 mM NaCl, where the system is fully nematic, is therefore likely a result of this effect. The calculations for Pf1 indicate that upon going from 30 mM to 500 mM salt, the order parameter of a rigid-rod fully aligned Pf1 liquid crystal decreases by about 8%. For comparison, Kassapidou et al. (1995) showed that for semi-flexible, fully aligned Na-DNA the order parameter decreases by about 15% when the NaCl concentration is increased from 90 mM to 500 mM (also assuming a Gaussian distribution function).

Alignment in isotropic phase

Below the isotropic coexistence concentration, the observed alignment is expected to scale with the square of the magnetic field strength. Alignment in this region is probed with the perdeuterated ubiquitin sample, which due to its electrostatic interaction with phage yields measurable dipolar couplings, even in the case of very dilute, weakly aligned Pf1. The presence of
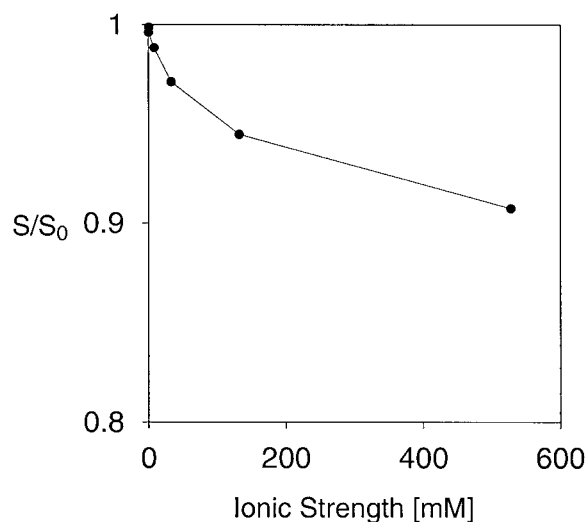
Figure 6. Theoretical ionic strength dependence of the ratio, S/S_0, of the Pf1 order parameter, S, and the Pf1 order parameter, S_0, at zero ionic strength. S was calculated from σ (Equation 7) assuming a Gaussian distribution, and σ was calculated based on the values of B_2c_p shown in Figure 1 (12 mg Pf1/ml), assuming rigid rods and neglecting the twist parameter h..

Figure 7. Magnetic field dependence of the ratio, S/S_n, of the Pf1 order parameter, S, in dilute Pf1, and the Pf1 order parameter, S_n, in the fully nematic phase. The S/S_n ratio is derived from the scaled ratio of the dipolar couplings measured for ubiquitin, 25 °C, 240 mM NaCl, pH 7.2 (see text). Open squares ($\square$) and filled squares ($\blacksquare$) correspond to Pf1 concentrations of 7.4 and 3.9 mg/ml, respectively. Dashed and dotted lines are linear fits to the data at 11.7 and 14.1 T, using $S = {}^2/_{15} \, \Delta\chi \, B_0^2/kT$, with $\Delta\chi$ the anisotropy of the diamagnetic susceptibility, B_0 the magnetic induction and kT the thermal energy (Bothner-By, 1996). The observed scaling with B_0 corresponds to apparent $\Delta\chi$ values of 54×10^{-30} m^3 at 7.4 mg Pf1/ml and 37×10^{-30} m^3 at 3.9 mg Pf1/ml. The solid line marks the expected order parameter as a function of B_0, using the previously reported value of $\Delta\chi = 15.3 \times 10^{-30}$ m^3 per Pf1 particle.

deuteration permits measurement of ^{15}N-^{1}H dipolar couplings for the majority of amides even in 20 mg/ml nematic Pf1, at 240 mM NaCl. If the order parameter in the nematic phase equals S_n, the Pf1 order, S, at low Pf1 concentrations is simply obtained from $S = (D^L/D^H) \times (P^H/P^L) \times S_n$, where D^L/D^H is the ratio of the ^{15}N-^{1}H dipolar couplings at low and high concentrations, and P^H/P^L is the ratio of the high and low Pf1 concentrations.

Figure 7 plots the Pf1 order measured in this manner as a function of the squared magnetic field strength. The solid line corresponds to the expected order parameter when using an anisotropic diamagnetic susceptibility, $\Delta\chi$, of 15.3×10^{-30} m^3 per Pf1 particle (Torbet and Maret, 1981). In contrast, even when using only 3.9 mg Pf1/ml and a high NaCl concentration of 240 mM, alignment of Pf1 is about two-fold higher than predicted on the basis of monomeric behavior. When increasing the Pf1 concentration to 7.4 mg/ml, which is right at the isotropic coexistence value, alignment of Pf1 particles is nearly three-fold higher relative to expected monomeric behavior. This suggests that even at these very low concentrations, alignment is not quite independent, or that a dynamic equilibrium between monomer, dimer and higher order multimers exists, similar to what was observed for magnetic alignment of porphyrins (Bothner-by et al., 1985).
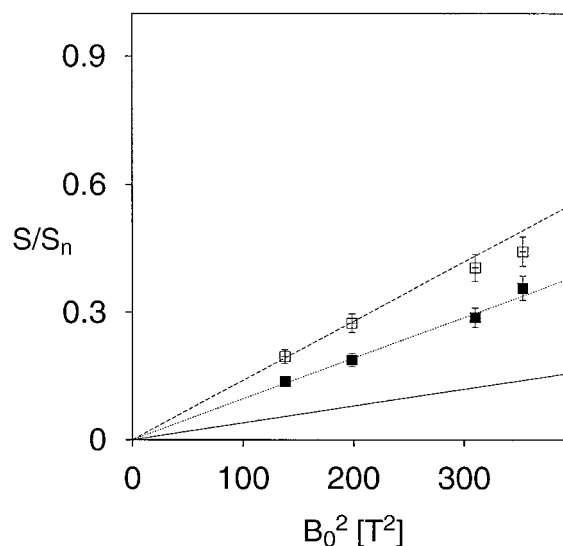
Temperature dependence of alignment

In isotropic solution, ordering of Pf1 particles is expected to be inversely proportional to temperature, and our measurements only provide indirect access to this alignment through either the ^{2}H quadrupole splitting, or through dipolar couplings in a dissolved macromolecule. The interaction between solvent or macromolecules and phage itself may be temperature dependent, and extracting the temperature dependence of phage alignment is therefore not straightforward. Below we base our analysis on the combined use of both the ^{2}H quadrupole splitting and dipolar couplings in solute macromolecules.

First, in agreement with an earlier report (Hansen et al., 2000), comparison of the ^{13}C-^{1}H dipolar couplings measured in a DNA oligomer in fully liquid crystalline Pf1 (26 mg/ml) at 25 and 7 °C shows only a minor ($12\pm2\%$) increase in alignment of the DNA fragment at the lower temperature. As both Pf1 and the oligomer are strongly negatively charged, little change
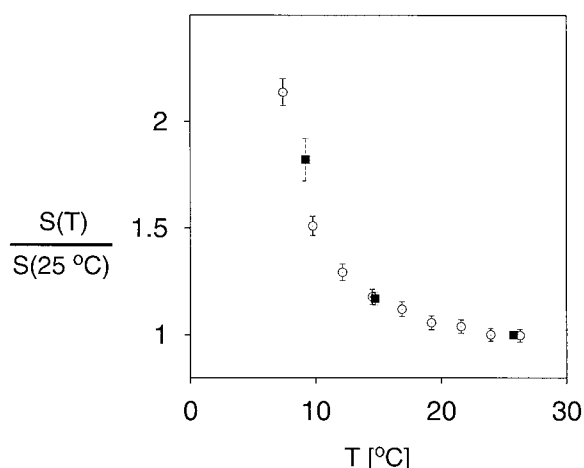
Figure 8. Temperature dependence of the Pf1 order parameter, as derived from ^{2}H quadrupole splittings (○) and from the alignment of ubiquitin (■) in a 3.9 mg/ml Pf1 solution, pH 7.2, 240 mM NaCl. See text for further details.

in the nature of the interaction between phage and the oligomer is expected in this temperature interval. The observed small increase in DNA alignment could result from several effects. It may be caused by a small increase in Pf1 order parameter, or it could indicate that the DNA dodecamer becomes effectively longer at the lower temperature because fraying at the ends of the oligomer decreases at lower temperature. The order of a solute in a constant electrostatic field will also increase at lower temperature because of the increase in the Boltzmann factor resulting from a decrease in kT. The Bjerrum length itself (Equation 4) will approximately stay unchanged because the increase in ε is largely offset by the decrease in kT.

In contrast to the dipolar couplings, the ^{2}H solvent quadrupole splitting decreases strongly (ca. 40%) when the temperature is reduced from 25 °C to 7 °C (Hansen et al., 2000). Considering that the degree of Pf1 alignment is comparable or slightly higher at the lower temperature, the decrease in ^{2}H splitting must be attributed to subtle changes in the average orientation of Pf1 hydration waters relative to the phage axis. A similar temperature dependence of the solvent ^{2}H splitting, without a concomitant change in protein order, has been noted in bicelle media (Ottiger and Bax, 1998) and has long been observed in oriented membranes (Finer and Darke, 1974).

Knowing how the ^{2}H splitting varies as a function of temperature for the fully aligned Pf1 sample, this information is used to scale the observed ^{2}H splitting at low Pf1 concentrations in order to obtain informa-

tion on the degree of alignment of dilute Pf1 samples. Figure 8 plots the ratio of the apparent Pf1 order parameter, derived from the appropriately scaled ^{2}H splitting, and the order parameter at 25 °C as a function of temperature for a dilute Pf1 sample (3.9 mg/ml; 240 mM NaCl). The same figure also shows the degree of Pf1 order as derived from the strength of ubiquitin's alignment. Both the ubiquitin data and the ^{2}H splitting derived Pf1 alignment indicate that for this dilute sample below the isotropic coexistence concentration, a reduction in temperature causes a strong increase in Pf1 alignment (Figure 8).

The change in Pf1 order parameter as a function of temperature points to a change in the Pf1 Δχ with temperature. Torbet and Maret observed an increase in the Cotton-Mouton constant by roughly a factor of two when the temperature was lowered from 20 °C to 5 °C (Torbet and Maret, 1981). As the Cotton-Mouton constant is a function of both the anisotropy of the diamagnetic susceptibility and the anisotropy of the optical polarizability, the change in the diamagnetic susceptibility alone could not be evaluated. The data in Figure 8 indicate that there is indeed a large increase in Δχ at low temperatures, and that the change in the Cotton-Mouton constant is dominated by the change in Δχ. In principle, the temperature dependence of the Pf1 order parameter could be caused by a change in alignment cooperativity as a function of temperature. However, this is unlikely to be the case as measurements at 3.9 mg Pf1/ml and lower ionic strength (100 mM NaCl) show the same dependence of the ^{2}H splitting on temperature (data not shown).

The variation of the diamagnetic susceptibility with temperature indicates that Pf1 undergoes a structural transition when the temperature is lowered from 25 to 7 °C. As the diamagnetic anisotropy arises principally from the α-helical peptide bonds, a change in average orientation of the α-helices of the major coat protein of Pf1 with respect to the virus long axis seems plausible (Torbet and Maret, 1981). Temperature-induced changes in Pf1 were also indicated by low-angle neutron scattering and X-ray fiber diffraction measurements (Torbet, 1979; Makowski et al., 1980).

Protein alignment in Pf1 at high ionic strength

Above 16 mg/ml, alignment of Pf1 is field-independent for $B_0 \geqslant 11.7$ T, up to 600 mM NaCl, indicating that the solution is fully nematic and Pf1 alignment is complete. However, at these high phage concentrations, frequently too much order is induced
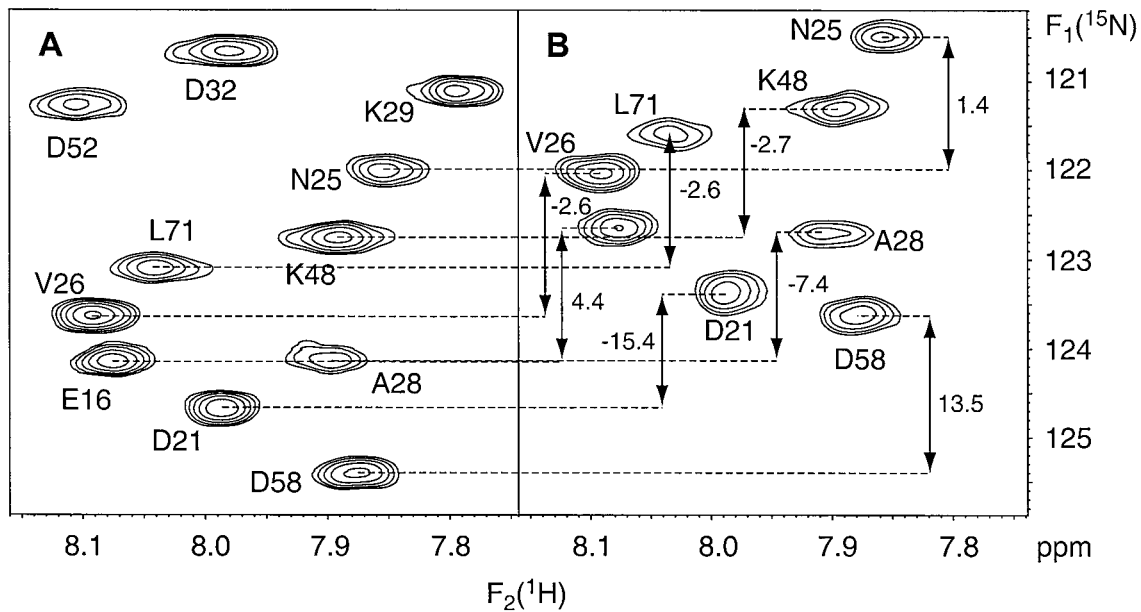
Figure 9. Small region of the IPAP [^{15}N, ^{1}H]-HSQC spectrum of ^{13}C/^{15}N-labeled ubiquitin, measured at 600 MHz in 19 mg/ml Pf1, 90% H$_2$O, 10% D$_2$O, 450 mM NaCl, pH 6.8, 25 °C. Downfield (A) and upfield (B) ^{15}N-{^{1}H} doublet components are shown separately. Changes in splitting relative to the isotropic ^{1}J$_{NH}$ values are marked in Hertz.

for macromolecules that have a significant electric dipole moment, rendering observation of rdc's by solution NMR difficult. Theoretical predictions of macromolecule alignment based on shape and charge distribution indicate that the degree of alignment induced by electrostatic interaction is a steep function of ionic strength (Zweckstetter et al., unpublished results). This is confirmed by experimental results. For example, at low ionic strength ubiquitin yields very strong alignment with dipolar couplings of several hundred Hz, and vanishing intensity for most of its resonances. In contrast, Figure 9 shows that when the salt concentration is increased to 450 mM at 19 mg/ml Pf1 (i.e., in the fully nematic phase), high quality spectra can be recorded. Only a modest degree of alignment remains, with ^{1}H-^{15}N dipolar couplings ranging from +25 to −18 Hz, and the dipolar couplings show good agreement (R = 0.99; Q = 0.17) with the NMR structure (Cornilescu et al., 1998), indicating that ubiquitin's structure is not affected by high ionic strength. The orientation of the alignment tensor of ubiquitin in Pf1 medium is very different from that in bicelles and the dipolar couplings in Pf1 provide important complementary information (data not shown) (Ramirez and Bax, 1998; Al-Hashimi et al., 2000).

Figure 10 shows the dependence of the ^{15}N T$_{1\rho}$ relaxation times for ^{2}H/^{13}C/^{15}N-enriched ubiquitin as
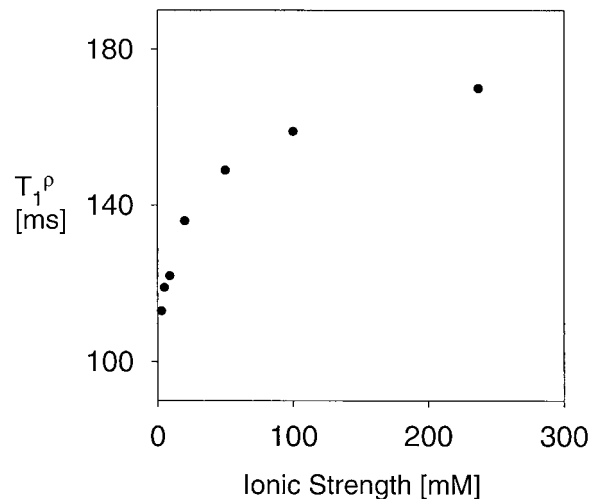

Figure 10. Average ^{15}N T$_{1\rho}$ relaxation times for ^{2}H/^{13}C/^{15}N-enriched ubiquitin as a function of ionic strength at 3.9 mg Pf1/ml, pH 7.2, 25 °C. Only ^{1}H^N resonances downfield from 8.5 ppm were included.

a function of ionic strength at 3.9 mg Pf1/ml. Due to the attractive electrostatic potential between Pf1 and ubiquitin and the hindered rotational diffusion when in the immediate vicinity of Pf1, ^{15}N T$_{1\rho}$ relaxation times of ubiquitin are significantly reduced at low salt concentrations, where the electrostatic interaction is
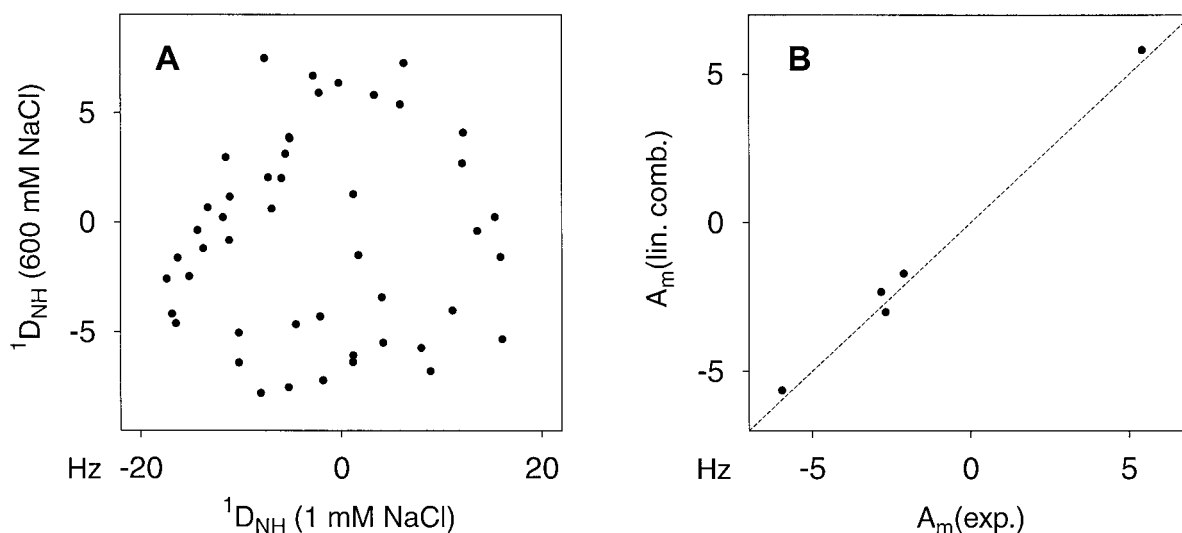
Figure 11. Comparisons of protein G alignment in different media. (A) $^1D_{NH}$ couplings at 1 mM NaCl versus those at 600 mM NaCl, both for 26 mg/ml Pf1, pH 7.2, 25 °C. (B) Components of the diagonalized protein G alignment tensor at 600 mM NaCl, A_m (exp.), versus a best-fit linear combination A_m(lin. comb.) of the alignment tensor in Pf1 at 1 mM NaCl and in 5% (w/v) DMPC/DHPC: A_m (lin. comb.) $= 0.41$ A_m(Pf1; 1 mM NaCl) $+ 0.53$ A_m (bicelle). For definition of A_m, see Sass et al. (1999).

least shielded. At 5 mM NaCl the average ^{15}N $T_{1\rho}$ is only 119 ms. With increasing ionic strength it approaches the isotropic value with a ^{15}N $T_{1\rho}$ of 175 ms at 240 mM NaCl. Increasing the Pf1 concentration to 26 mg/ml at a constant pH and 240 mM salt concentration decreases the average ^{15}N $T_{1\rho}$ to 110 ms. The increase in Pf1 concentration raises the fraction of ubiquitin close to Pf1, thereby reducing its rotational diffusion and $T_{1\rho}$ relaxation time. These data indicate that it is advantageous to increase both the Pf1 concentration and the ionic strength for measurement of dipolar couplings in proteins that tend to align too much. The ^{15}N $T_{1\rho}$ at 240 mM NaCl and 26 mg Pf1/ml is about the same as at 3.9 mg Pf1/ml and 5 mM NaCl. However, the degree of alignment of ubiquitin is about three times higher at 26 mg Pf1/ml than at 3.9 mg/ml. Therefore, for the same degree of protein alignment one has improved relaxation properties at high Pf1 and high salt concentrations, despite the higher intrinsic viscosity of water at high ionic strength. Of course, exceptions to this rule can occur too. For example, one may expect increased aggregation for hydrophobic proteins at high ionic strength, in which case dipolar couplings must be measured at low Pf1 concentrations and low ionic strength. In this case, when working below the nematic Pf1 threshold concentration, the highest available field strength is desirable in order to maximize Pf1 alignment.

Multiple alignment tensors in Pf1

Residual dipolar couplings in proteins can readily be observed in a Pf1 medium at low ionic strength when electrostatic repulsion and steric obstruction are the dominant interactions (Hansen et al., 2000). For such systems, increasing the ionic strength will weaken the electrostatic interaction, but leave the steric effect unchanged, thereby providing yet another method for modulating the alignment tensor. As an example, Figure 11A compares $^1D_{NH}$ splittings in protein G at low and high ionic strength. Residual dipolar couplings at 600 mM NaCl are almost completely uncorrelated with those at 1 mM NaCl. The two corresponding order matrices, obtained by singular value decomposition from the observed dipolar couplings, are at a generalized angle (Sass et al., 1999) of 74°. It is interesting to note that the dipolar couplings at low and high salt fit equally well to the X-ray structure (Gallagher et al., 1994). The strong change in the orientation of the alignment tensor is caused by an increased influence of the electrostatic component at low ionic strengths. Indeed, as shown in Figure 11B, the alignment tensor at 600 mM NaCl can be expressed as a linear combination of the alignment tensor at low ionic strength in Pf1 and that in nearly neutral bicelles, where alignment is completely steric (Zweckstetter and Bax, 2000). This agrees with results reported for

ubiquitin alignment in a dilute suspension of charged purple membrane fragments (Sass et al., 1999).

Concluding remarks

At low ionic strength Pf1 solutions remain fully nematic down to very low concentrations of a few mg/ml. However, both theoretical and experimental results indicate that the nematic threshold concentration shifts significantly with increasing ionic strength, and increases up to ca. 16 mg/ml for a NaCl concentration of 600 mM. Remarkably, there is no abrupt decrease in Pf1 order below the nematic threshold. Instead, the system becomes paranematic between the isotropic and anisotropic coexistence concentrations. In this region, Pf1 alignment depends strongly on the magnetic field strength. However, Pf1 alignment remains considerably higher than expected for monomeric behavior, by a factor that depends on how far the concentration decreases below the nematic threshold.

Working at a phage concentration below the nematic threshold strongly reduces the degree of induced alignment for a solute macromolecule relative to what would be expected if the medium were to remain nematic. However, the contribution to the transverse relaxation rate for a solute protein resulting from transient interaction with the phage scales linearly with phage concentration, regardless of the degree of phage alignment. So, although the dipolar couplings can readily be scaled down to the desired range by diluting the phage concentration, the increased transverse relaxation resulting from the presence of Pf1 may remain significant.

The nematic threshold concentration for Pf1 is approximately two-fold lower than for *fd*, whereas the surface electrostatic properties are quite similar. Therefore, it is expected that for proteins that have a net electrostatic attraction to Pf1 and *fd*, working with Pf1 is preferred because lower Pf1 concentrations (in mg/ml) can induce the same degree of alignment at a smaller cost in increased relaxation.

Alignment of dilute, isotropic Pf1 solutions increases nearly two-fold when the temperature is lowered from 25 to 5 °C. Although this results in increased alignment of the solute macromolecule, increased solvent viscosity at lower temperature largely offsets the gain from this increased alignment.

For macromolecules whose alignment is not entirely dominated by electrostatic interactions, varying the ionic strength provides yet another mechanism to modulate the orientation and magnitude of the alignment tensor. This may prove particularly useful in ongoing work to determine protein structures from dipolar couplings in the absence or near-absence of NOE information (Delaglio et al., 2000; Hus et al., 2000).

References

Al-Hashimi, H.M., Valafar, H., Terrell, M., Zartler, E.R., Eidsness, M.K. and Prestegard, J.H. (2000) *J. Magn. Reson.*, **143**, 402–406.

Barrientos, L.G., Louis, J.M. and Gronenborn, A.M. (2001) *J. Magn. Reson.*, **149**, 154–158.

Bothner-By, A.A. (1996) In *Encyclopedia of Nuclear Magnetic Resonance*, Vol. 5 (Grant, D.M. and Harris, R.K., Eds), Wiley, Chichester, pp. 2932–2938.

Bothner-by, A.A., Gayathri, C., Vanzijl, P.C.M., Maclean, C., Lai, J.J. and Smith, K.M. (1985) *Magn. Reson. Chem.*, **23**, 935–938.

Cavagnero, S., Dyson, H.J. and Wright, P.E. (1999) *J. Biomol. NMR*, **13**, 387–391.

Clore, G.M. and Garrett, D.S. (1999) *J. Am. Chem. Soc.*, **121**, 9008–9012.

Clore, G.M., Starich, M.R. and Gronenborn, A.M. (1998) *J. Am. Chem. Soc.*, **120**, 10571–10572.

Cornilescu, G., Marquardt, J.L., Ottiger, M. and Bax, A. (1998) *J. Am. Chem. Soc.*, **120**, 6836–6837.

Delaglio, F., Grzesiek, S., Vuister, G.W., Zhu, G., Pfeifer, J. and Bax, A. (1995) *J. Biomol. NMR*, **6**, 277–293.

Delaglio, F., Kontaxis, G. and Bax, A. (2000) *J. Am. Chem. Soc.*, **122**, 2142–2143.

Dogic, Z. and Fraden, S. (1997) *Phys. Rev. Lett.*, **78**, 2417–2420.

Finer, E.G. and Darke, A. (1974) *Chem. Phys. Lipids*, **12**, 1–16.

Fleming, K., Gray, D., Prasannan, S. and Matthews, S. (2000) *J. Am. Chem. Soc.*, **122**, 5224–5225.

Gallagher, T., Alexander, P., Bryan, P. and Gilliland, G.L. (1994) *Biochemistry*, **33**, 4721–4729.

Gronenborn, A.M., Filpula, D.R., Essiz, M.Z., Achari, A., Whitlow, M., Wingfield, P.T. and Clore, G.M. (1991) *Science*, **253**, 657–661.

Hansen, M.R., Hanson, P. and Pardi, A. (2000) *Methods Enzymol.*, **317**, 220–240.

Hansen, M.R., Rance, M. and Pardi, A. (1998) *J. Am. Chem. Soc.*, **120**, 11210–11211.

Hanus, J. (1969) *Phys. Rev. Lett.*, **178**, 420.

Herzfeld, J., Berger, A.E. and Wingate, J.W. (1984) *Macromolecules*, **17**, 1718–1723.

Hus, J.C., Marion, D. and Blackledge, M. (2000) *J. Mol. Biol.*, **298**, 927–936.

Kassapidou, K., Heenan, R.K., Jesse, W., Kuil, M.E. and Vandermaarel, J.R.C. (1995) *Macromolecules*, **28**, 3230–3239.

Khokhlov, A.R. and Semenov, A.N. (1981) *Physica*, **A108**, 546–556.

Khokhlov, A.R. and Semenov, A.N. (1982) *Macromolecules*, **15**, 1272–1277.

Khokhlov, A.R. and Semenov, A.N. (1982) *Physica*, **A112**, 605–614.

Kostrikis, L.G., Liu, D.J. and Day, L.A. (1994) *Biochemistry*, **33**, 1694–1703.

Lekkerkerker, H.N.W., Coulon, P., Vanderhaegen, R. and Deblieck, R. (1984) *J. Chem. Phys.*, **80**, 3427–3433.

Liu, D.J. and Day, L.A. (1994) *Science*, **265**, 671–674.

Makowski, L., Caspar, D.L.D. and Marvin, D.A. (1980) *J. Mol. Biol.*, **140**, 149–181.

Manning, G.S. (1987) *Biopolymers*, **26**, 1–3.

Odijk, T. (1986) *Macromolecules*, **19**, 2314–2329.

Oldenbourg, R., Wen, X., Meyer, R.B. and Caspar, D.L.D. (1988) *Phys. Rev. Lett.*, **61**, 1851–1854.

Ojennus, D.D., Mitton-Fry, R.M. and Wuttke, D.S. (1999) *J. Biomol. NMR*, **14**, 175–179.

Onsager, L. (1949) *Ann. NY Acad. Sci.*, **51**, 627–659.

Ottiger, M. and Bax, A. (1998) *J. Biomol. NMR*, **12**, 361–372.

Ottiger, M. and Bax, A. (1999) *J. Biomol. NMR*, **13**, 187–191.

Ottiger, M., Delaglio, F. and Bax, A. (1998) *J. Magn. Reson.*, **131**, 373–8.

Peng, J.W., Thanabal, V. and Wagner, G. (1991) *J. Magn. Reson.*, **94**, 82–100.

Ramirez, B.E. and Bax, A. (1998) *J. Am. Chem. Soc.*, **120**, 9106–9107.

Ramirez, B.E., Voloshin, O.N., Camerini-Otero, R.D. and Bax, A. (2000) *Protein Sci.*, **9**, 2161–2169.

Ruckert, M. and Otting, G. (2000) *J. Am. Chem. Soc.*, **122**, 7793–7797.

Sanders, C.R. and Schwonek, J.P. (1992) *Biochemistry*, **31**, 8898–8905.

Sass, J., Cordier, F., Hoffmann, A., Cousin, A., Omichinski, J.G., Lowen, H. and Grzesiek, S. (1999) *J. Am. Chem. Soc.*, **121**, 2047–2055.

Sato, T. and Teramoto, A. (1991) *Physica*, **A176**, 72–86.

Skrynnikov, N.R., Goto, N.K., Yang, D.W., Choy, W.Y., Tolman, J.R., Mueller, G.A. and Kay, L.E. (2000) *J. Mol. Biol.*, **295**, 1265–1273.

Song, L., Kim, U.-S., Wilcoxon, J. and Schurr, J.M. (1991) *Biopolymers*, **31**, 547–567.

Stigter, D. (1977) *Biopolymers*, **16**, 1435.

Stigter, D. (1982) *Macromolecules*, **15**, 635–641.

Stroobants, A., Lekkerkerker, H.N.W. and Odijk, T. (1986) *Macromolecules*, **19**, 2232–2238.

Tang, J.X. and Fraden, S. (1993) *Phys. Rev. Lett.*, **71**, 3509–3512.

Tang, J.X. and Fraden, S. (1995) *Liquid Cryst.*, **19**, 459–467.

Tang, J.X. and Fraden, S. (1996) *Biopolymers*, **39**, 13–22.

Tjandra, N. and Bax, A. (1997) *Science*, **278**, 1111–1114.

Tjandra, N., Omichinski, J.G., Gronenborn, A.M., Clore, G.M. and Bax, A. (1997) *Nat. Struct. Biol.*, **4**, 732–738.

Tjandra, N., Tate, S., Ono, A., Kainosho, M. and Bax, A. (2000) *J. Am. Chem. Soc.*, **122**, 6190–6200.

Tolman, J.R., Flanagan, J.M., Kennedy, M.A. and Prestegard, J.H. (1995) *Proc. Natl. Acad. Sci. USA*, **92**, 9279–9283.

Torbet, J. (1979) *FEBS Lett.*, **108**, 61–65.

Torbet, J. and Maret, G. (1981) *Biopolymers*, **20**, 2657–2669.

Vroege, G.J. (1989) *J. Chem. Phys.*, **90**, 4560–4566.

Vroege, G.J. and Odijk, T. (1988) *Macromolecules*, **21**, 2848–2858.

Zimmermann, K., Hagedorn, H., Heuck, C.C., Hinrichsen, M. and Ludwig, H. (1986) *J. Biol. Chem.*, **261**, 1653–1655.

Zweckstetter, M. and Bax, A. (2000) *J. Am. Chem. Soc.*, **122**, 3791–3792.